Journal of
Applied Crystallography

ISSN 0021-8898

Received 15 September 2008
Accepted 5 February 2009

Formalism for the determination of intermediate stress gradients using X-ray diffraction

Thomas Gnäupel-Herold

University of Maryland, Department of Materials Science and Engineering, College Park, MD 20742, USA, and NIST Center for Neutron Research, 100 Bureau Drive Stop 6102, Gaithersburg, MD 20899-6102, USA. Correspondence e-mail: tg-h@nist.gov

A method is outlined that allows the determination of one-dimensional stress gradients at length scales greater than 0.2 mm. By using standard four-circle X-ray diffractometer equipment and simple aperture components, length resolutions down to 0.05 mm in one direction can be achieved through constant orientation of a narrow, line-shaped beam spot. Angle calculations are given for the adjustment of goniometer angles, and for the effective azimuth and tilt of the scattering vector for general angle settings in a four-circle goniometer. The latter is necessary for the computation of stresses from lattice strain measurements.

1. Introduction

Stress determination using X-ray diffraction is based on measuring lattice spacings in different directions within a chosen specimen reference frame. This is performed experimentally by tilting (angle ψ) and rotating (angle φ) the specimen with respect to the incident and the diffracted X-ray beam. X-ray diffraction is predominantly surface limited owing to the strong absorption of X-rays in most materials, and the resulting penetration depths are of the order of micrometres. Stress gradients with significant changes within the penetration depth can be determined (Genzel, 1994, 1999); however, the evaluation of strain/stress gradients for length scales much larger than the penetration depth is mostly limited to neutron diffraction, synchrotron X-ray diffraction and laboratory X-ray diffraction in connection with layer removal.

Neutron diffraction is commonly used with spatial resolutions $\geq$1 mm but measurements with resolutions of 0.1 mm have been reported (Foecke & Gnaupel-Herold, 2006; Gnaeupel-Herold *et al.*, 2004; Oliveira *et al.*, 2006). Unless new focusing optics become available (Gibson *et al.*, 2002) further improvements are unlikely owing to limitations of the primary beam intensity. Synchrotron X-ray diffraction offers primary beam intensities superior both to neutron diffraction and to laboratory X-ray diffraction. It has been used successfully to determine strain and stress gradients at all length scales ranging from 10^{-3} to 10^{-1} mm (Larson *et al.*, 2002; Gnaeupel-Herold *et al.*, 2005; Jakobsen *et al.*, 2006; Levine *et al.*, 2006; Martinschitz *et al.*, 2008; Rahman *et al.*, 2008). However, availability and cost limit the widespread use of both techniques. Thus, the most common diffractive method for the determination of intermediate stress gradients is laboratory X-ray diffraction in connection with electrochemical layer removal from the surface (Suominen & Carr, 2000). Although layer removal is a destructive method which causes perturbations of the stress field, there is often no alternative.

In this work a different approach is outlined, based on measuring the lattice spacings on the cross-sectional surface using collimated beams in a diffraction geometry that minimizes or keeps constant the size and location of the spot of the incident beam. This is implemented in two different modes, one in which the width of the beam spot stays constant and one in which the spot width varies. The angle calculations governing the diffraction geometries are derived.

2. Diffraction geometry

For the following considerations, biaxial stress states are assumed with no contributions for all normal components σ_{i3}. For the sake of simplicity, it is also implied that the sample is elastically isotropic. First and foremost, high spatial resolution (in one dimension) requires (1) excellent beam definition, (2) close proximity of the primary beam aperture to the specimen

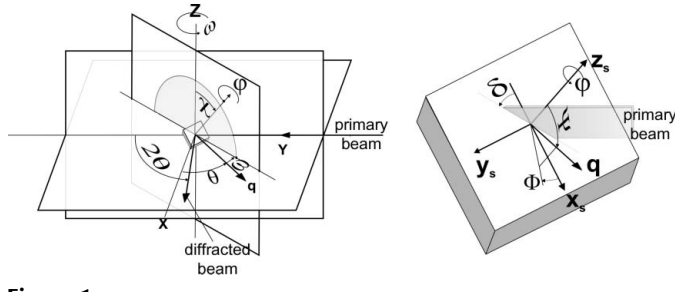

Figure 1
Diffraction geometry in a four-circle configuration. The primary beam should be pictured as rectangular, and it is within the *YZ* plane (typical beam dimensions Z = 3 mm, X = 0.04 mm). On the right, the magnified specimen is shown. The z_s axis is parallel to the φ axis. The azimuth Φ is the angle between $\mathbf{x}_s$ and the normal projection of the scattering vector $\mathbf{q}$ onto the specimen surface. The tilt Ψ is the angle between $\mathbf{z}_s$ and $\mathbf{q}$. The angle δ introduced here is the rotation of the beam spot at φ = constant with respect to $(\omega + \theta) = 90^\circ$ where $\delta = 0$.

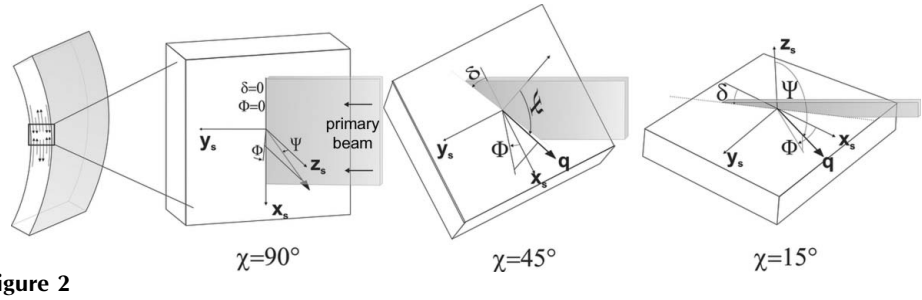

Figure 2
Left: schematic example of a through-thickness stress field that can be determined with the technique described in this work. Right: magnified measurement field with rotation δ of the beam spot as the specimen (left) is tilted with χ at $(\omega + \theta) \neq 90^\circ$. The beam-spot size is minimal at $(\omega + \theta) = 90^\circ$.

and (3) low beam divergence. Requirements (1) and (2) can be easily fulfilled through simple collimator tubes with attached slits; for (3) it is sufficient to use fine-focus X-ray tubes with focal spot sizes of 0.4 mm. For example, in a routinely used experimental setup the aperture to specimen distance was 30 mm, the focal spot to specimen distance was 350 mm and the aperture size was 0.04 × 3 mm. The spatial resolution was evaluated through moving a specimen into the beam and measuring the background-corrected integral intensity, resulting in a measured resolution of 0.05 mm. In order to translate the beam definition (dimensions) into constant spatial resolution at all tilt angles, the proposed diffraction geometry requires combinations of tilt, azimuth and ω rotation angles that can be produced only in a four-circle goniometer (Fig. 1).

The naming of angles follows that given in the classic treatment of four-circle geometry by Busing & Levy (1967). In order to avoid conflicts between the naming of Euler rotations (ω, χ, φ) and the commonly used names for the azimuth and tilt angle of the scattering vector in the specimen reference frame, the capitalized letters Φ (azimuth) and Ψ (tilt) are used, as shown in Fig. 2. With all diffractometer angles set to zero, the specimen frame from Fig. 2 coincides with the laboratory frame from Fig. 1. The angle θ is the Bragg angle from the equation

$$\lambda = 2d_{hkl} \sin\theta \qquad (1)$$

in which λ is the wavelength, hkl are the Miller indices and d_{hkl} is the lattice spacing. Two strategies/geometries exist in conventional diffraction-based lattice strain measurements. In the omega mode, the specimen tilt is performed such that the scattering vector is within the scattering plane (*i.e.* the axis of rotation is perpendicular to the scattering plane), and

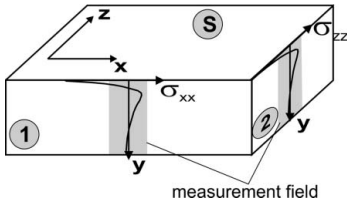

Figure 3
Accessibility of gradients of in-plane stresses from side surfaces. Note that the same reference frame is used for all three surfaces, which causes each normal component to have a different index x, y, z.

rectangular beams are often employed. The use of measurements with defined spatial resolution is limited because the orientation of the spot is constant but not its width, which increases with $1/\cos\Psi$ (Wilson, 1963). This broadening of the beam spot creates complex correlations between the tilt angle and the spatial distribution of lattice strains.

In the psi mode, the scattering vector tilts perpendicularly to the scattering plane, *i.e.* the tilt axis is within the scattering plane. The beam is usually circular or quadratic in cross section, and both the size and the orientation of the spot change. In both the omega and the psi modes the stress tensor components can be separated by choosing specimen orientations with $\Phi = 0^\circ$ or $\Phi = 90^\circ$ as follows from equation (2) (see Noyan & Cohen, 1987; Hauk, 1997):

$$\begin{aligned}\varepsilon_{\Phi\Psi}(hkl) = (1/2)\, s_2(hkl)\,[&(\sigma_{11}\cos^2\Phi + \sigma_{22}\sin^2\Phi + \sigma_{12}\sin 2\Phi)\\ &\times \sin^2\Psi + \sigma_{33}\cos^2\Psi + (\sigma_{13}\cos\Phi + \sigma_{23}\sin\Phi)\\ &\times \sin 2\Psi] + s_1(hkl)(\sigma_{11} + \sigma_{22} + \sigma_{33}).\end{aligned} \qquad (2)$$

The use of the geometry shown in Fig. 1 for residual stress determination has been described in the literature (Reimers, 1992; Hauk, 1997; Welzel *et al.*, 2005), and it is similar to the psi method with omega tilt described by Hauk (1997), where equations are derived for a transformation equivalent to equation (2). The equations given by Hauk (1997) can be omitted through the expressions for Φ and Ψ derived in the following. Similar expressions for Φ and Ψ were also given by Welzel *et al.* (2005). It should be noted that the rotation δ of the beam spot occurs at all angles $\chi \neq 90^\circ$ and $(\omega + \theta) \neq 90^\circ$ in addition to any sample rotation φ.

For the following considerations, it is assumed that (1) the stresses involving the surface normal component are zero within the X-ray penetration depth and (2) within the measurement field the stresses are constant in one direction. The reference frame used here is defined in Fig. 3.

An example of such a stress field is found in the homogeneous (constant radius of curvature) bending of a sheet. Conditions (1) and (2) are also fulfilled for many types of two-dimensional deformations and the resulting plane stresses such as deformed membranes (deep-drawn sheet metal) or deep-reaching (> 1 mm depth) peening stresses. For example, the changes of the stress component σ_{xx} in the **y** direction can be measured on surface (1) and the **y** dependence of component σ_{zz} can be measured on surface (2). Stresses caused by shallow (comparable to the X-ray penetration depth) two-dimensional surface deformations do not fall into this category because the stress in the in-plane direction that becomes the surface normal on a side surface is subject to relaxations [σ_{zz} on surface (1)]. For measurements on the surfaces (1) and (2) it is assumed that the measurement field is

sufficiently small and there is sufficient distance from the edges for the stresses to be unaffected by the left and right edges. If the stresses change in both directions within the beam-spot area [for example, if σ_{xx} changes in both the **x** and the **y** directions on surface (1)], then the length of the beam spot on the specimen surface has to be decreased such that $\sigma_{xx} \simeq$ constant within the length of the beam spot in this direction. This can be done either through a smaller X-ray beam or by means of thin (< 10 μm) lead foils attached to the specimen surface such that the illuminated area is constant as suggested by the rectangular measurement field in Fig. 2 (left). Thus, in order to evaluate the change of the stresses σ_{xx} in the **y** direction, the primary X-ray beam has to be shaped such that it forms a beam spot long in the **x** direction and narrow in the **y** direction. The *xy* dimensions of the beam spot are derived from the requirements of spatial resolution for a particular stress field. The orientation of the beam spot has to be kept constant in order to maintain the spatial resolution at each tilt angle. It should be noted that edge effects need to be avoided, as depicted by using only the middle region of the specimen in Fig. 2. For example, σ_{xx} becomes zero at both the upper and the lower edges.

A constant orientation of the beam spot on the specimen surface requires that the φ angle is adjusted by δ as outlined in Fig. 2. The adjustment can be calculated from the intersection of the *YZ* plane in the laboratory reference frame and the specimen surface, given by the two vectors $\mathbf{x}_s$ and $\mathbf{y}_s$ (see Fig. 1). Using the transposed **R** matrix (see Busing & Levy, 1967), all four vectors can be expressed in the specimen frame [the phi frame of Busing & Levy (1967)] in terms of instrument angles:

$$\mathbf{Y} = \tilde{\mathbf{R}} \begin{pmatrix} 0 \\ -1 \\ 0 \end{pmatrix} = \begin{bmatrix} \sin(\omega+\theta)\cos\chi\cos\varphi + \cos(\omega+\theta)\sin\varphi \\ \sin(\omega+\theta)\cos\chi\sin\varphi - \cos(\omega+\theta)\cos\varphi \\ \sin(\omega+\theta)\sin\chi \end{bmatrix}, \tag{3}$$

$$\mathbf{Z} = \tilde{\mathbf{R}} \begin{pmatrix} 0 \\ 0 \\ 1 \end{pmatrix} = \begin{pmatrix} -\sin\chi\cos\varphi \\ -\sin\chi\sin\varphi \\ \cos\chi \end{pmatrix}. \tag{4}$$

At $\varphi = 0$, $\mathbf{x}_s$ and $\mathbf{y}_s$ become

$$\mathbf{x}_s = \begin{pmatrix} 1 & 0 & 0 \end{pmatrix}^{\mathrm{T}}, \tag{5}$$

$$\mathbf{y}_s = \begin{pmatrix} 0 & 1 & 0 \end{pmatrix}^{\mathrm{T}}, \tag{6}$$

from which the following expression for the angle δ is derived:

$$\delta = \pm \arccos\Big([\cos\chi\sin(\omega+\theta) + \sin\chi\tan\chi\sin(\omega+\theta)] \Big/ \big\{ \cos^2(\omega+\theta) + [\cos\chi\sin(\omega+\theta) + \sin\chi\tan\chi\sin(\omega+\theta)]^2 \big\}^{1/2} \Big). \tag{7}$$

Note that $(\theta + \omega)$ is the total specimen rotation, *i.e.* one has symmetric diffraction at $\omega = 0$. The following quadrant convention applies:

$$\delta < 0 \begin{cases} 0^\circ < (\theta+\omega) < 90^\circ, & 0^\circ < \chi < 90^\circ, \\ 90^\circ < (\theta+\omega) < 180^\circ, & 90^\circ < \chi < 180^\circ, \end{cases} \tag{8a}$$

$$\delta < 0 \begin{cases} 0^\circ < (\theta+\omega) < 90^\circ, & 90^\circ < \chi < 180^\circ, \\ 90^\circ < (\theta+\omega) < 180^\circ, & 0^\circ < \chi < 90^\circ. \end{cases} \tag{8b}$$

The angle δ is independent on φ which is why φ can be set to zero for the purpose of calculating δ. Equation (2) is not defined for $\chi = 90^\circ$ but from Fig. 2 it is obvious that $\delta = 0$ for $\chi = 90^\circ$. The angle δ is an additional rotation of φ, *i.e.* it is additive, and is independent of the actual orientation of the primary beam. For example, equation (2) is also correct if the plane of the primary beam is chosen such that it is parallel to the *XY* plane.

If left uncorrected, the changing orientation of the beam spot on the specimen would be equivalent to measuring the lattice spacings over a larger effective area given by the beam dimensions. In effect, a smoothing of the stress gradient takes place. The effective increase *b* of the beam spot with χ and ω is shown in Fig. 4.

By adjusting φ at every Ψ tilt, the size of the beam spot remains unchanged as well (at large Ψ angles, the part of the beam spot further away from the apertures may become broader as a result of divergence). Thus, the constant orientation and size of the beam spot make measurements with high resolution actually feasible. The resolution is only limited by the closeness of the beam apertures and the beam divergence, as well as the willingness to accept the necessary data acquisition times.

A constant orientation of the beam spot has the consequence that the tilt plane is inclined against the specimen surface (Fig. 5). Thus, the azimuth Φ and tilt Ψ are generally not identical to φ and $(90^\circ - \chi)$, respectively. This tilt mode and the equations for Φ and tilt Ψ have been described in the literature (Hauk, 1997; Welzel *et al.*, 2005); however, new expressions for Φ and Ψ are developed to allow for the

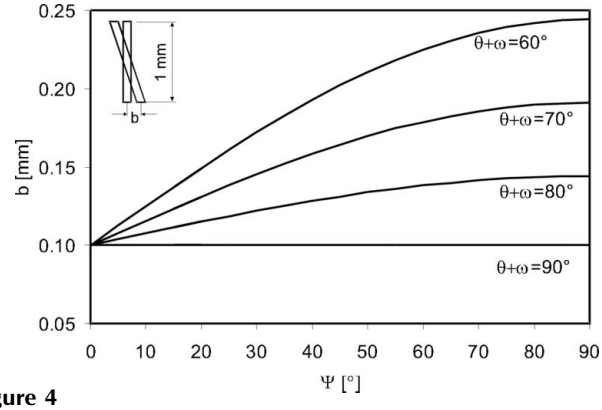

Figure 4
The rotation of the rectangular beam spot due to changing orientation of the specimen with Ψ. The result is an effective broadening *b*. It is assumed that the beam spot is 0.10 mm wide in the **X** direction of the laboratory system and 1.0 mm high in the **Z** direction. The broadening is proportional to the height of the beam, *e.g.* a 2.0 mm beam will produce twice the broadening. The lengthening of the beam spot with Ψ is disregarded because it can be easily limited through a lead foil window attached to the specimen surface. The graphs were calculated using equation (2).

different reference frames used, and to include the correction δ. Both Φ and Ψ can be calculated using the transformations described by Busing & Levy (1967) by expressing the vectors $\mathbf{q}$, $\mathbf{x}_s$, $\mathbf{y}_s$ and $\mathbf{z}_s$, in terms of instrument angles. Ψ is the angle between the surface normal (assumed to be parallel to the φ axis) and the scattering vector $\mathbf{q}$,

$$\mathbf{q} = \tilde{\mathbf{R}}\begin{pmatrix}1\\0\\0\end{pmatrix} = \begin{pmatrix}\cos\omega\cos\chi\cos\varphi - \sin\omega\sin\varphi\\ \cos\omega\cos\chi\sin\varphi + \sin\omega\cos\varphi\\ \cos\omega\sin\chi\end{pmatrix}. \quad (9)$$

The matrix $\mathbf{R}$ is given explicitly by Busing & Levy (1967). One obtains for Ψ

$$\cos\Psi = \cos\omega\sin\chi. \quad (10)$$

With the correction δ applied, Φ is the angle between the projection of $\mathbf{q}$ on to the $x_s y_s$ plane and the vector $\mathbf{x}_s$:

$$\cos\Phi = \frac{[\cos\omega\cos\chi\cos(\varphi+\delta) - \sin\omega\sin(\varphi+\delta)]}{(\cos^2\omega\cos^2\chi + \sin^2\omega)^{1/2}}. \quad (11)$$

Equations (10) and (11) allow the calculation of azimuth and tilt for any specimen orientation. If the orientation of the beam spot is not of interest then one can set $\delta = 0$. The symmetric case is where $\omega = 0$ corresponds to the psi mode and one has $\varphi + \delta = \Phi$ and $\cos\Psi = \sin\chi$. In the omega mode, one has $\chi = 90^\circ$ and $\cos\Phi = -\sin(\varphi + \delta)$. The latter is the result of the choice of axes here and it represents an offset of $\pi/2$, *i.e.* $\Phi = \pi/2 + \varphi + \delta$.

3. Strategies for high spatial resolution

3.1. General considerations

If the intensity of the primary beam was abundant, one would simply choose aperture settings that give the primary beam the necessary dimensions to provide a defined spatial/area resolution on the specimen. This is not the case for conventional X-ray sources, and one has to compromise by having good spatial resolution only in one dimension while the aperture in the perpendicular direction remains as far open as possible to provide both sufficient diffracted intensity and good grain statistics. The latter is a result of the beam-spot area being less than 1 mm^2 which, for large-grained materials, reduces significantly the number of grains contributing to a particular diffraction peak at a given orientation. According to the simple scheme used by Gnaeupel-Herold *et al.* (2004) for a grain number calculation, one can estimate that for typical experimental settings the total number of grains in a reflecting orientation is of the order of 1 (linear position-sensitive detector with 2° vertical opening, 10 µm penetration depth, grain size 20 µm, 0.10 × 5 mm beam). Such low grain numbers almost always require the use of oscillations in ω and χ in order to improve the grain statistics. The grain statistics are essential for stress determination because they affect not only the accuracy of the measurement of the lattice spacing but also the validity of the underlying assumptions about polycrystal elastic behavior (Luzin *et al.*, 2002). In the above example the average number of grains contributing to one peak can be increased to more than 20 by using $\Delta\chi = \pm 2^\circ$ oscillation in χ and $\Delta\omega = \pm 5^\circ$ oscillation in ω (1° interval, determined from a single grain rocking curve). The δ correction is performed at each oscillation $\Delta\chi$ and $\Delta\omega$. If necessary, and if the specimen geometry allows, the statistics can be improved further through shifting of the measurement field (*e.g.* along the **x** direction in Fig. 2).

Although the spatial resolution can be calculated from the aperture settings and then beam divergence, the effective spatial resolution should be verified because of the possible misalignment of the beam spot with a specimen reference direction (*i.e.* the edge of the specimen should be parallel to the line-shaped beam spot). This is done experimentally though an edge scan in which the specimen is moved incrementally into the beam. The integrated intensity of a reflection increases as more of the specimen surface is illuminated, and the slope of this function is used to evaluate the effective spatial resolution [see Wang *et al.* (1998) for the treatment of neutron beams].

3.2. Constant orientation/minimum size beam spot

Two modes of operation exist in which the small beam-spot dimension stays both constant in orientation and at its smallest

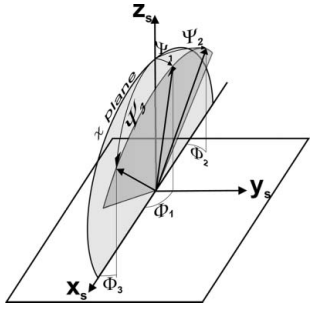

Figure 5
The meaning of Φ and Ψ for an arbitrary tilt scan in the specimen reference frame. The psi mode is a tilt within the χ plane at $\omega = 0$; the omega mode (not shown) is within the $y_s z_s$ plane with $\chi = 90^\circ$. Each orientation of the scattering vector produces combinations (Ψ_1,Φ_1; Ψ_2,Φ_2; Ψ_3,Φ_3 . . .) in which Φ changes together with Ψ.

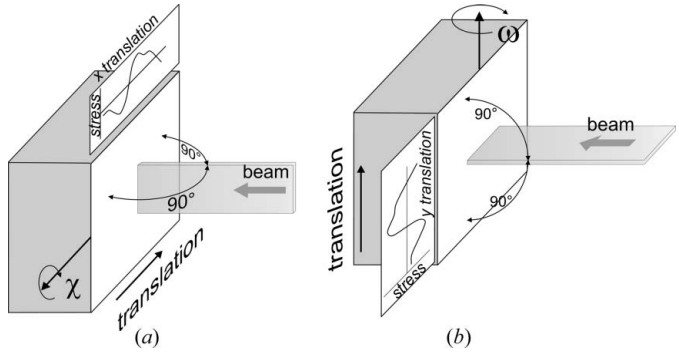

Figure 6
Tilt-scan options for a constant orientation and a minimum beam spot. For both tilts the plane of the primary beam given by its height/width directions is always perpendicular to the specimen surface. (*a*) χ tilt, (*b*) ω tilt.

possible size in a tilt scan: one by setting $(\omega + \theta) = 90^\circ$ and one by keeping $\chi = 90^\circ$. This is outlined in Fig. 6. The specimen surface and the primary beam plane are perpendicular to each other. The Ψ–Φ motion is produced either through the χ circle (Fig. 6*a*) or through the ω rotation (Fig. 6*b*). The main difference between Figs. 6(*a*) and 6(*b*) is that in Fig. 6(*a*) the scattering vector is not parallel to the tilt plane because it would require $\theta = 90^\circ$ and $\omega = 0$. $\theta = 90^\circ$ implies perfect backscattering and it is experimentally impossible.

The χ tilt yields tupels (Ψ, Φ) in which both depend on (ω, χ, φ) through equations (10) and (11). From equation (2) and Fig. 5, it follows that stress tensor components cannot be separated in this mode. However, as implied earlier, the formalism requires that, within the length of the beam spot, the stress field is constant in the direction of the long dimension of the beam spot. Thus, this component can be determined from an omega-mode measurement.

The ω tilt in Fig. 6(*b*) produces scans in which (Ψ, Φ = constant) which allows the selective measurement of stress tensor components (in Fig. 6: σ_{11}). It should be noted that often the χ tilt (Fig. 6*b*) is preferable to the ω tilt (Fig. 6*b*) because of superior resolution $\Delta\theta/\tan\theta$ due to the small size of the beam spot within the scattering plane. Therefore, the ω tilt in Fig. 6(*b*) should only be used if a χ rotation is not available or if the selective measurement of stress tensor components is required with $\Phi = 0^\circ$ or $\Phi = 90^\circ$.

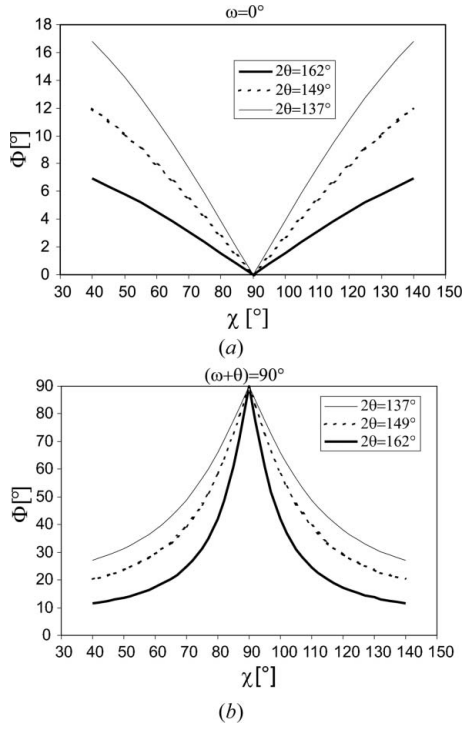

Figure 7
Effective azimuth angle Φ for a χ-tilt scan with $\omega = 0$ (*a*) and for the geometry shown in Fig. 6(*a*) with $(\omega + \theta) = 90^\circ$ (*b*). The angle φ was set to $\varphi = 0$ which makes $\Phi = \delta$ in (*a*). In (*b*), one obtains for the correction $\delta = 0$. Note that in (*a*) the tilt angle $\Psi = \chi - 90^\circ$.

3.3. Constant orientation/minimum azimuth variation

The measurement geometries in Fig. 6 are preferable if the smallest possible beam spot is a priority. An alternative can be found in the symmetric mode similar to Fig. 6(*a*) with the exception that $\omega = 0$. The symmetric mode differs from the psi mode only by the correction δ applied to φ at every angle χ. As shown in Fig. 7 the variation of the effective azimuth Φ (including the correction δ) is much smaller for $\omega = 0$ than for $(\omega + \theta) = 90^\circ$. For large values of 2θ the angle Φ is sufficiently small to allow the selective evaluation of stress tensor components, *i.e.* by setting $\Phi = 0^\circ$ or $\Phi = 90^\circ$.

4. Discussion

The non-destructive evaluation of gradients of in-plane stress fields up to ~1 mm depth/thickness has been frequently challenging because of the scarcity of suitable experimental resources (synchrotron, neutron sources). The approach presented here circumvents many of the difficulties associated with the evaluation of these stress fields by measuring the depth dependence of the lattice strains, not from the surface by means of penetration radiation, but from the side of a specimen using a well collimated beam of weakly penetrating X-rays. The need for a fixed orientation of a line-shaped beam spot creates complex relationships between specimen orientation and the directions of the measured strains. This, in turn, mostly prohibits a simplistic data analysis such as linear regression of lattice strain *versus* $\sin^2\psi$. As a result, explicit assumptions have to be made about stress tensor components or additional measurements have to be performed in different directions Φ. The first approach can be used for many problems in which boundary conditions permit only negligibly small stresses in one direction. Also, symmetric scans with $\omega = 0$ and intermediate tilts (see Fig. 7*a*) permit only small contributions by σ_{22} and σ_{12}.

The capabilities of a four-circle goniometer are another requirement for the implementation of this technique. The limits of applicability, *i.e.* a stress gradient can be measured in only one direction and resolutions of ~0.05 mm, still include a wide variety of materials problems such as sheet metal formation, laminated structures and layers, certain surface treatments such as laser peening or shot peening, and the study of edge effects. A notable advantage of the method is that X-ray goniometers with the necessary capabilities are widely available, thus providing a simpler way of studying the aforementioned class of residual stress problems.

References

Busing, W. R. & Levy, H. A. (1967). *Acta Cryst.* **22**, 457–464.
Foecke, T. & Gnaupel-Herold, T. (2006). *Metall. Mater. Trans. A*, **37**, 3503–3510.
Genzel, C. (1999). *J. Appl. Cryst.* **32**, 770–778.
Genzel, Ch. (1994). *Phys. Status Solidi A*, **146**, 629–637.
Gibson, W. M., Schultz, A. J., Chen-Mayer, H. H., Mildner, D. F. R., Gnäupel-Herold, T., Miller, M. E., Prask, H. J., Vitt, R., Youngman, R. & Carpenter, J. M. (2002). *J. Appl. Cryst.* **35**, 677–683.
Gnaeupel-Herold, T., Prask, H. J., Fields, R. J. & Foecke, T. J. (2005). *Mater. Sci. Eng. A*, **399**, 26–32.

Gnaeupel-Herold, T., Prask, H. J., Fields, R. J., Foecke, T. J., Xia, Z. C. & Lienert, U. (2004). *Mater. Sci. Eng. A*, **366**, 104–113.
Hauk, V. (1997). Editor. *Structural and Residual Stress Analysis by Nondestructive Methods*. Amsterdam: Elsevier Science.
Jakobsen, B., Poulsen, H. F., Lienert, U., Almer, J., Shastri, S. D., Sørensen, H. O., Gundlach, C. & Pantleon, W. (2006). *Science*, **312**, 889–892.
Larson, B. C., Yang, W., Ice, G. E., Budai, J. D. & Tischler, J. Z. (2002). *Nature* (*London*), **415**, 887–890.
Levine, L. E., Larson, B. C., Yang, W., Kassner, M. E., Tischler, J. Z., Delos-Reyes, M. A., Fields, R. J. & Liu, W. (2006). *Nat. Mater.* **5**, 619–622.
Luzin, V., Gnäupel-Herold, T. & Prask, H. J. (2002). *Mater. Sci. Forum*, **408–412**, 407–412.
Martinschitz, K. J., Kirchlechner, C., Daniel, R., Maier, G., Mitterer, C. & Keckes, J. (2008). *Mater. Sci. Forum*, **571–572**, 101–106.
Noyan, I. C. & Cohen, J. B. (1987). *Residual Stress Measurement by Diffraction and Interpretation*. New York: Springer.
Oliveira, M. C., Baptista, A. J., Alves, J. L., Menezes, L. F., Green, D. E., Gnaeupel-Herold, T., Iadicola, M. A., Foecke, T. & Stoughton, T. B. (2006). Proceedings of the International Deep-Drawing Research Group Conference, Porto, Portugal, 19–21 June, pp. 279–286.
Rahman, M., Fitzpatrick, M. E., Edwards, L., Pratihar, S., Peel, M., Steuwer, A. & Buslaps, T. (2008). *Mater. Sci. Forum*, **571–572**, 119–124.
Reimers, W. (1992). *Measurement of Residual and Applied Stress Using Neutron Diffraction*, edited by H. T. Hutchings & A. D. Kravitz, pp. 159–170. Dordrecht: Kluwer Academic Publishers.
Suominen, L. & Carr, D. (2000). *Adv. X-ray Anal.* **43**, 21–30.
Wang, X.-L., Spooner, S. & Hubbard, C. R. (1998). *J. Appl. Cryst.* **31**, 52–59.
Welzel, U., Ligot, J., Lamparter, P., Vermeulen, A. C. & Mittemeijer, E. J. (2005). *J. Appl. Cryst.* **38**, 1–29.
Wilson, A. J. C. (1963). *Mathematical Theory of X-ray Powder Diffractometry*. Eindhoven: Philips Technical Library.